Effects of Short-Range Forces on the Lone-Range Structure of Hydrous Iron Oxide Aggregates

ARTICLE *in* LANGMUIR · JANUARY 1989

Impact Factor: 4.46 · DOI: 10.1021/la00085a036

2 AUTHORS:

Vincent A. Hackley
National Institute of Standards and Technology
111 PUBLICATIONS **2,097** CITATIONS
SEE PROFILE

Anderson Marc
University of Wisconsin–Madison
56 PUBLICATIONS **3,367** CITATIONS
SEE PROFILE

adsorbs in $d_{0.7}$ and half-filled $d_{1.18}$ pores. From Figure 7, one can see that this analysis nicely explains why each dye molecule excludes twice its molecular area.

Criticism of the Microporosity Analyses. When the adsorption process is pore filling, the t-plot method is inapplicable because the concept of the thickness t of an adsorbed film is inappropriate. However, Atkinson et al. and Marsh proposed that the process of micropore filling is initially by surface coverage and then by cooperative adsorption.[6,19] The theoretical calculation of interaction potential in a slit-shaped pore of ca. $3d_N$ width indicated that an adsorbate molecule is likely to adsorb on walls of micropores.[18] Recently, we also found that the adsorption process in slitlike micropores is by monolayer coverage and subsequent pore filling or multilayer adsorption.[2,20] We believe, therefore, that the t-plot method gives some measure of the micropore size distribution, although, strictly speaking, t should be replaced by the corrected value determined by taking account enhanced adsorption energy.[21]

The Innes method gives an outline of the micropore size distribution (Figure 4), in spite of the limitation due to use of the Kelvin equation. Whenever the method is applied to a type I isotherm we can obtain a pore size distribution curve which seems to be consistent with the t-plot, although the maximum porosity is somewhat larger than that from the t-plot.

Both the t-plot and the Innes method demonstrate that the pore volume is reduced to zero with preadsorption, whereas the pore width remains essentially constant (Figures 3 and 4). This result is consistent with the maximum of porosity in the range 0.7 – 0.84 nm as concluded from the preadsorption method (Table III). When preadsorption of dye occurs in $d_{0.7}$ pores, N_2 molecules are excluded in proportion to adsorbed dye (Figure 7); i.e., the pore volume decreases and the pore width remains unchanged as long as porosity is determined by N_2 adsorption.

Conclusions

We have examined the surface and pore structure of ACF by the dye adsorption. The preadsorption method with a dye is proposed in order to estimate the fractal structure and the (micro)pore size distribution of porous solids. These methods gave an apparent fractal dimension and micropore size distribution for ACF. For fractal analysis, the size of probe molecules preadsorbed must be smaller than the surface roughness. For estimation of the pore size distribution, however, the probes should be comparable with the pore radius. From this point of view, OII molecules seem to be suitable for the latter purpose but not the former since ACF has micropores of width less than 1.0 nm. Clearly, when probe molecules and adsorbent are properly selected, the power of the method is enhanced.

Registry No. OII, 633-96-5; AR88, 1658-56-6; MB, 61-73-4; CV, 548-62-9; PcB, 147-14-8; AR27, 915-67-3; NG, 19381-50-1.

(19) Marsh, H. *Carbon* **1987**, *25*, 49.
(20) Kakei, K.; Suzuki, T.; Ozeki, S.; Kaneko, K. *Colloids Surf.*, submitted.
(21) Brunauer, S. *Proceedings of International Symposium Surface Area Determination*; Everett, D. H.; Ottewill, R. H., Eds.; Butterworths: London, 1970; p 63.

Effects of Short-Range Forces on the Long-Range Structure of Hydrous Iron Oxide Aggregates

Vincent A. Hackley* and Marc A. Anderson

Water Chemistry Program, University of Wisconsin, 660 North Park St., Madison, Wisconsin 53706

Received August 1, 1988. In Final Form: October 7, 1988

The salt-induced aggregation of colloidal goethite (α-FeOOH) is investigated by using quasi-elastic, static, and electrophoretic light-scattering methods. Stability measurements, based on initial rates of aggregation, define distinct reaction- (RL) and diffusion- (DL) limited kinetic regimes, with the transition occurring at the critical coagulation concentration. Electrophoretic mobility and ζ potential show a similar transition region. The static structure factor $S(q)$, determined from the angular dependence of scattered intensity, has a power law form that reflects long-range density correlations for the aggregates, consistent with a fractal structure. The scattering exponent yields an effective fractal dimension of 1.6 and 2.0 for DL and RL regimes, respectively. The DL dimensionality is significantly lower than previously measured experimental values for systems involving spherical geometries. This effect may be a consequence of anisotropic sticking, which has been observed to induce ordering through face-to-face orientation of platelike primary goethite particles. A simple model involving short-range DLVO interactions is suggested to account for this behavior.

Introduction

In light of the numerous studies pertaining to colloidally dispersed metal oxides, surprisingly little is known about their aggregated state, although the latter certainly plays a significant role in determining many of the physicochemical properties of suspensions.[1-3] In 1979 Forrest and Witten[4] first observed long-range power law density correlations in vapor-phase aggregates of iron, zinc, and silica, which yielded power law exponents close to 1.8. The results of this study indicated a similarity between the problem of aggregation and the scale-invariant properties of critical systems such as percolation[5] and second-order

* Author to whom correspondence should be addressed.

(1) Anderson, M. A.; Tejedor-Tejedor, M. I.; Stanforth, R. R. *Environ. Sci. Technol.* **1985**, *19*, 632.
(2) Witten, T. A.; Cates, M. E. *Science* **1986**, *232*, 1607.
(3) Lindsay, H. M.; Lin, M. Y.; Weitz, D. A.; Sheng, P.; Chen, Z.; Klein, R.; Meakin, P. *Faraday Discuss. Chem. Soc.* **1987**, *83*, 153.
(4) Forrest, S. R.; Witten, T. A., Jr. *J. Phys. A: Math. Gen.* **1979**, *12*, L109.

0743-7463/89/2405-0191$01.50/0

phase transitions.[6] In critical phenomena, the power law exponent reflects an effective dimensionality associated with a type of structural symmetry in which the characteristic fluctuations or geometric features remain unchanged under spatial dilation. Mandelbrot[7] has shown that dilation symmetry is a common attribute of many natural formations (e.g., Brownian paths, river networks, coast lines, and the distribution of galaxies), and he has popularized the term "fractal" for such objects.

The initial work of Forrest and Witten kindled a renewed interest in chaotic, nonequilibrium kinetic growth processes, for which fractal behavior is a manifestation. Long-range structural correlations have since been identified in a variety of particle aggregates, although the primary emphasis has been on computer-simulated kinetic growth models,[8] which have increased greatly our understanding of the mechanisms and controlling factors involved in the formation of nonequilibrium structures. In the current study, our objective is to apply these concepts to the problem of colloidal aggregation in metal oxide systems.

Hydrous ferric oxides are geochemically important components[9-11] in many soil and aquatic systems and are of interest in a variety of industrial processes, for instance, as corrosion products[12] or precursors for magnetic memory systems.[13] The hydrous oxyhydroxide goethite (α-FeOOH) is frequently used[14-19] as a model colloid for studying interfacial adsorption reactions and testing electrostatic double-layer models. The available body of knowledge, and the ability to synthesize goethite in different sizes and shapes[20] makes it an excellent choice for investigating particle aggregation and the effects of short-range interactions and particle anisotropy on structure. Colloidal goethite is electrostatically stabilized in aqueous suspension by the adsorption of potential determining H^+ and OH^- ions at the surface and is positively charged below the isoelectrc point (measured at pH 9 ± 0.5 for particles used in this study). Aggregation can be induced by changing the pH, adding a flocculating agent such as phosphate, or increasing the electrolyte concentration until the surface charge is screened.

In an earlier paper, Van der Woude et al.[21] propose that the flat-faced morphology of their synthesized goethite is responsible for a "string-like ordering" of flocs they observe and that this behavior is more apparent at low electrolyte concentrations, due to repulsive interactions between primary particles. We believe that the observed string-like ordering is, at least in part, a result of fractal growth (kinetic control). In addition, we differentiate between short-range (particle–particle) structure and long-range (fractal) structure in our interpretation of aggregate formation, although the two regimes are not mutually exclusive. We build upon and extend the previous work of Van der Woude et al. in our analysis of a similar system, while emphasizing the effects of short-range interaction forces.

In this paper we report on an investigation of the salt-induced aggregation of goethite at constant pH. From elastic light-scattering measurements, the aggregates appear to have long-range fractal correlations. We have integrated the structural analysis with measurements of colloidal stability and electrokinetic behavior determined from quasi-elastic and electrophoretic light scattering, respectively. We employ fractal concepts to quantitatively characterize the long-range structure of these aggregates, and we compare our results to model simulations. In all equations, standard SI units apply unless otherwise noted.

Theory

Measuring Particle Size. The process of transformation from stable suspension to aggregated state is generally characterized by the loss of primary particles at the expense of larger clusters and is accompanied by an increase in mean particle size. We use photon correlation spectroscopy (PCS), a quasi-elastic light-scattering (QELS) technique, to measure particle size in situ. In PCS, a suspension of particles is illuminated by a laser, and the time-dependent scattered photon signal is measured and autocorrelated. The measured autocorrelation function ($G(\tau)$) is then fit to an equation of the general form[22-24]

$$G(\tau) = B[1 + C|g^1(\tau)|^2] \quad (1)$$

where B is the base line value and is proportional to the square of the time-averaged intensity, C is an instrument constant, τ is the delay time, and $g^1(\tau)$ is the first-order autocorrelation function. For a monodisperse system of dilute, optically isotropic (or small relative to the incident wavelength, i.e., a Rayleigh scatterer), noninteracting particles, $g^1(\tau)$, determined from eq 1, is directly related to the translational diffusion coefficient D_T:[23]

$$|g^1(\tau)| = \exp(-D_T q^2 \tau) \quad (2)$$

$$\Gamma = D_T q^2 \quad (3)$$

where Γ is the decay constant, $q = 4\pi n \sin(\theta/2)/\lambda$ is the momentum transfer in units of reciprocal length, n is the refractive index of the medium, θ is the scattering angle, and λ is the vacuum wavelength of incident light.

Polydisperse systems are analyzed by using the method of cumulants[25] in which a distribution of exponential terms in $g^1(\tau)$ is assumed:

$$|g^1(\tau)| = \int_0^\infty F(\Gamma) \exp(-\Gamma\tau)\, d\Gamma \quad (4)$$

where $F(\Gamma)$, the distribution function, is expanded in a power series of τ. The first moment (cumulant) in the expansion is the average decay constant, Γ_{avg}, which defines

(5) Stanley, H. E. *J. Phys. A: Math. Gen.* **1977**, *10*, L211.
(6) Wegner, F. J. In *Critical Phenomena*; Brey, J., Jones, R. B., Eds.; Lecture Notes in Physics; Springer-Verlag: New York, 1976; Vol. 54, pp 2–19.
(7) Mandelbrot, B. B. *The Fractal Geometry of Nature*; W. H. Freeman: New York, 1983.
(8) Meakin, P. In *On Growth and Form, Fractal and Non-Fractal Patterns in Physics*; Stanley, H. E., Ostrowsky, N., Eds.; Proc. NATO ASI Ser., Ser. E, No. 100; Martinus Nijhoff: Dordrecht, Netherlands, 1986; pp 111–135.
(9) Hingston, F J.; Posner, A M.; Quirk, J. P. *J. Soil Sci.* **1974**, *25*, 16.
(10) Waite, T. D.; Morel, F. M. M. *Environ. Sci. Technol.* **1984**, *18*, 860.
(11) Sigg, L.; Stumm, W. *Colloids Surf.* **1981**, *2*, 101.
(12) Kaneko, K.; Inouye, K. *Bull. Chem. Soc. Jpn.* **1979**, *52*, 315.
(13) Inouye, K.; Shibata, K.; Ozeki, S.; Kaneko, K. *J. Electrochem. Soc.* **1984**, *131*, 2435.
(14) Jurinak, J. J. *J. Colloid Sci.* **1964**, *19*, 477.
(15) Onoda, G. Y., Jr.; de Bruyn, P. L. *Surf. Sci.* **1966**, *4*, 48.
(16) Machesky, M. L.; Anderson, M. A. *Langmuir* **1986**, *2*, 582.
(17) Zhang, Y.; Kallay, N.; Matijevic, E. *Langmuir* **1985**, *1*, 201.
(18) Penners, N. H. G.; Koopal, L. K.; Lyklema, J. *Colloids Surf.* **1986**, *21*, 457.
(19) Zeltner, W. A.; Anderson, M. A. *Langmuir* **1988**, *4*, 469.
(20) Atkinson, R. J.; Posner, A. M.; Quirk, J. P. *J. Inorg. Nucl. Chem.* **1968**, *30*, 2371.
(21) Van der Woude, J. H. A.; Rijnbout, J. B.; de Bruyn, P. L. *Colloids Surf.* **1984**, *11*, 391.
(22) Ford, N. C. In *Measurement of Suspended Particles by Quasi-Elastic Light Scattering*; Dahneke, B E., Ed.; Wiley: New York, 1983; Chapter 2.
(23) Pecora, R. In *Measurement of Suspended Particles by Quasi-Elastic Light Scattering*; Dahneke, B. E., Ed.; Wiley: New York, 1983; Chapter 1.
(24) Morrison, I. D.; Grabowski, E. F.; Herb, C. A. *Langmuir* **1985**, *1*, 496.
(25) Koppel, D. E. *J. Chem. Phys.* **1972**, *57*, 4814.

an effective diffusion coefficient, D_{eff}, for the particle (or aggregate) distribution. We convert D_{eff} to an effective hydrodynamic radius, r_H, using the Stokes–Einstein relationship[26]

$$D_{eff} = \frac{kT}{6\pi\eta r_H} \tag{5}$$

where η is the viscosity of the medium, k is the Boltzmann constant, and T is the absolute temperature of the experiment.

The effects of polydispersity fluctuations, minor "dust" contamination, and hydrodynamic interactions are reduced by performing size determinations in the high-q region[27] ($\theta \approx 90$–$120°$). High-q measurements on anisotropic particles, however, may include contributions to the decay constant from rotational diffuson[28] and must be considered in the interpretation of PCS data.

Determination of Colloid Stability. In the present study we use PCS to measure the initial rate of salt-induced aggregate growth. From this kinetic data we determine a stability factor (W) which is calculated in the manner outlined by Novich and Ring.[28,29] The subsequent stability analysis is based in part on relationships derived by Reerink and Overbeek[30] in accordance with the Derjaguin–Landau–Verwey–Overbeek (DLVO) theory of stability.[31] The initial aggregation rate is described by a second-order rate equation[32]

$$-\left.\frac{dN}{dt}\right|_{t=0} = k_R N_0^2 \tag{6}$$

Here k_R is the Smoluchowski second-order rate constant for rapid (diffusion-limited) aggregation and N_0 is the initial particle number concentration at time zero. In the presence of an electrostatic repulsive barrier, the aggregation rate is retarded by a factor $1/W$, where $W = k_R/k_S$ is termed the stability ratio and k_S is the slow (reaction-limited) rate constant. Experimentally, we measure the initial rate of change of r_H, which is proportional to the left-hand term in eq 6, and normalize all values to the highest rate while correcting for different N_0.

We apply the parallel flat-plate, constant surface potential version of the DLVO stability model,[31] the assumptions of which we find to be generally consistent with our experimental system: flat-plate geometry with preferred face-to-face association for primary particles (based on electron microscopic observations and previous work[21]). According to DLVO, the total pair interaction potential (U) is the algebraic sum of electrostatic repulsive (+) and van der Waals attractive (−) potentials:

$$U = U_A + U_R \tag{7}$$

We use an approximate expression for U_R as a function of the half-distance of separation (h) between parallel surfaces:

$$U_R = \frac{64 n_0 kT}{\kappa}\gamma^2 \frac{\exp(-2\kappa h)}{1+\exp(-2\kappa h)} S \tag{8}$$

where n_0 is the number concentration of ions in the bulk solution, κ is the Debye–Hückel parameter characterizing the reciprocal thickness of the electrical double layer (a function of both electrolyte concentration and valence), and S is the area of interaction between the two parallel plates. The unitless variable γ is a Gouy–Chapman–Stern[26] double-layer electrostatic parameter defined as

$$\gamma = \left[\exp\left(\frac{ze\psi_S}{2kT}\right) - 1\right] \Big/ \left[\exp\left(\frac{ze\psi_S}{2kT}\right) + 1\right] \tag{9}$$

where e is the electron charge, z is the counterion valence, and ψ_S is the Stern potential. The parameter ψ_S is not directly obtainable; however, the ζ potential (ζ), determined from electrokinetic measurements, is an acceptable approximation for many colloidal systems.[26,33,34] In using this approximation one assumes that the shear plane associated with ζ is located at or near the specific adsorption (Stern) plane close to the particle surface, beyond which lies a diffuse layer of counterions and co-ions obeying a Poisson–Boltzmann distribution with an exponential decay in potential.

We calculate U_A from

$$U_A = -\frac{A_{212}}{48\pi}\left[\frac{1}{h^2} + \frac{1}{(h+\delta)^2} - \frac{2}{(h+\delta/2)^2}\right] S \tag{10}$$

where A_{212} is the goethite/H_2O/goethite Hamaker constant characterizing the strength of dipole–dipole interactions between plates of thickness δ.

For a specific iron oxide sol at a fixed pH and temperature, U is a function of electrolyte concentration (C_E) and z and may take on + or − values depending on the separation distance and the degree of ionic screening. Reerink and Overbeek[30] showed that W, and therefore colloid stability, is determined primarily by the height of the electrostatic repulsive barrier (U_{max}) such that

$$W \propto \exp(U_{max}/kT) \tag{11}$$

and, holding all other variables constant, a linear relationship exists between log W and log C_E. The critical coagulation concentration (CCC) marks the onset of diffusion-limited kinetics and is determined by extrapolation to log $W = 0$ in a logarithmic plot of W versus C_E. An effective A_{212} can be calculated from stability data by using the above-mentioned approximation for ψ_S and the following expression,[31] derived for the case of flat-plate interactions when $U_{max} = 0$:

$$\text{CCC (mol·L}^{-1}) = 87.4 \times 10^{-40}(\gamma^4/z^6 A_{212}^2) \tag{12}$$

Structural Analysis. In contrast to QELS, static light scattering (SLS) is used as an in situ probe of the internal structure of colloidal aggregates. The geometric arrangement of primary particles of size r, in a cluster of size R, leads to interference in the scattered waves, much as X-rays are diffracted by planes in a crystal lattice. Information about the internal arrangement of primary particles is therefore contained in the structure factor ($S(q)$), which is the Fourier transformation of the pair correlation function. The parameter q is in units of reciprocal length, and by altering q (changing the scattering angle) we are effectively altering the scale of observation and probing correlations of varying length. When $qr > 1$ the primary particle form factor dominates the spectrum, and when $qR < 1$ we can no longer resolve details of the internal structure of the clusters. Between these two limits, $S(q)$ is dominated by particle–particle correlations within

(26) Hiemenz, P. C. *Principles of Colloid and Surface Chemistry*, 2nd ed.; Marcel Dekker: New York, 1986.
(27) Pusey, P. N.; Tough, R. J. A. In *Dynamic Light Scattering*; Pecora, R., Ed.; Plenum: New York, 1985; Chapter 4.
(28) Novich, B. E.; Ring, T. A. *Clays Clay Miner.* **1984**, *32*, 400.
(29) Novich, B. E.; Ring, T. A. *J. Chem. Soc., Faraday Trans. 1* **1985**, *81*, 1455.
(30) Reerink, H.; Overbeek, J. Th. G. *Faraday Discuss. Chem. Soc.* **1954**, *18*, 74.
(31) Verwey, E. J. W.; Overbeek, J. Th. G. *Theory of the Stability of Lyophoic Colloids*; Elsevier: New York, 1948.
(32) Smoluchowski, M. v. *Z. Physik. Chem. (Leipzig)* **1917**, *92*, 129.
(33) Overbeek, J. Th. G. *J. Colloid Interface Sci.* **1977**, *58*, 408.
(34) Enustun, B. V.; Turkevich, J. *J. Am. Chem. Soc.* **1963**, *85*, 3317.

the aggregates. For a fractal object, the long-range correlations in structure result in a power law dependency for $S(q)$:[35,36]

$$I(q) \sim S(q) \sim q^{-x} \quad (13)$$

where $I(q)$ is the scattered intensity and x is the scattering exponent. A structural analysis depends on the interpretation of x and therefore requires a scaling law to establish the relationship between mass (probed by $I(q)$) and the length scale (reciprocal q):[7,35]

$$M(L) \sim L^D; \ 1 \leq D \leq d \quad (14)$$

Equation 14 describes the spatial distribution of mass (M) within a mass-fractal object as a function of length scale (L) with a characteristic exponent D, the fractal dimension. D is a measure of how closely packed the primary particles are within a cluster, and typically one finds $D \leq d$, where d is the spatial (Euclidian) dimension in which the fractal object is embedded. If $D = d$, the cluster is a solid object with distinct boundaries and a constant mass density. If $D < d$, then the cluster is ramified with a density that decreases as the length scale of measurement increases.

Equation 14 contains the essential elements of eq 13 necessary to interpret the scattering exponent: $I(q)$ is proportional to the average mass within $1/q$ distance of any particle center, and scaling arguments show[35,37] that $x = D$ in the power law domain. The slope of a logarithmic plot of I versus q gives D directly. Martin[38] has shown that x can also depend on the polydispersity exponent (τ_P) for power law polydisperse systems, although for $\tau_P < 2$ the scattering exponent is unaffected. Diffusion-limited aggregation (DLA) is characterized by a peaked distribution of cluster sizes;[39] however, the reaction-limited mode of aggregation (RLA) is expected to yield a power law distribution. Model simulations[40,41] indicate that for RLA $\tau_P \leq 2$ and that for relativey small rigid clusters $\tau_P \approx 1.5$. Experiments on colloidal gold aggregates[39,42] give $\tau_P = 1.5$, while Martin[43] found $1.85 \leq \tau_P \leq 2$ for silica aggregates. These results are consistent with current models and suggest that polydispersity is not a factor in the determination of x for these systems. Additionally, in both RLA and DLA thelargest clusters dominate the scattering profile,[42] reducing the effects of polydispersity on x caused by the presence of smaller clusters[35] in the distribution.

Experimental Section

Colloidal goethite (α-FeOOH) was prepared[16] in polypropylene containers by neutralization and subsequent aging of a ferric nitrate solution (ACS reagent grade chemicals), according to a procedure by Atkinson et al.[20] The solid was washed repeatedly with ultrapure Milli-Q H_2O by sedimentation and decantation until a constant supernatant conductivity of 5 $\mu S \cdot cm^{-1}$ was reached. The solid was then freeze-dried and stored as a desiccated powder. The N_2 BET surface area was measured as 81 $m^2 \cdot g^{-1}$, and powder X-ray diffraction confirmed the solid to be crystalline goethite. A stock suspension of 90 $mg \cdot L^{-1}$ was then prepared by ultrasonic dispersion of the powder in Milli-Q H_2O adjusted to pH 4 with HNO_3 (ultrex grade) in a polycarbonate container. The suspension was then allowed to settle for several days and decanted, and the supernatant was passed through a 0.6-μm pore size Nuclepore filter to remove dust and large aggregates. The final suspension was allowed to equilibrate for months prior to analysis, with no appearance of visible sediment over a 1-year period.

Goethite crystallizes in an orthorhombic lattice with unit cell dimensions $a_0 = 4.6$ Å, $b_0 = 10.0$ Å, and $c_0 = 3.03$ Å.[44] From transmission electron microscopy (TEM) we find the primary particle to be a single crystal having, at low resolution, a plate-like morphology with approximate proportions 60 nm × 18 nm × 11 nm. It is believed the predominant face is the (100) crystallographic plane, while the crystals are known to elongate in the (001) direction.[44,45] We measure an effective hydrodynamic radius of 39 ± 2 nm by using QELS and find this value to be insensitive to ionic strength in the range 0.0001–0.08 $mol \cdot L^{-1}$ $NaNO_3$ (aggregation interferes with this determination above 0.08) and to be independent of scattering angle in the range 30–160°. For purposes of identification, we refer henceforth to goethite of this particular geometry simply as G2. SLS and QELS measurements were performed on a Brookhaven Model BI200SM servomotor-controlled light-scattering goniometer with a Model BI2030 64-channel digital autocorrelator (Brookhaven Instruments, Holtsville, NY). The incident light source was a 10-mW He–Ne laser (Melles Griot, Los Angeles, CA) operating at a 632.8-nm wavelength with vertical polarization. We carried out all sample preparation in a Liberty Model 4003 laminar-flow clean air station (Liberty Industries, East Berlin, CT) in order to reduce dust contamination to an insignificant level for light-scattering measurements.

Particle electrophoretic mobility and specific conductance measurements were made on a PenKem system 3000 electrokinetics analyzer (PenKem, Inc., Bedford Hills, NY) equipped with a cylindrical electrophoresis cell.

Extinction measurements were made on a Varian DMS 80 UV–vis spectrophotometer (Varian instrument division, Palo Alto, CA) with a 1-cm quartz cell and a slit width setting of 0.2 nm to reduce stray and forward scattered light.

Experiments were performed at 25 °C under strict temperature control. The general experimental procedure was as follows. All stock solutions were adjusted to pH 4 with HNO_3, followed by filtration through a 0.2-μm Nuclepore filter. An appropriate volume of $NaNO_3$ solution was placed in cell 1 to give the desired final electrolyte concentration. An aliquot of suspension was added to cell 2 and Milli-Q H_2O added to both cells as necessary for dilution. Cell volumes were approximately equal. At time zero cell 1 was emptied into cell 2, and the contents of cell 2 then poured back into cell 1 and finally returned to cell 2 in order to assure complete mixing. Cell 2 was then placed in the goniometer, and we measured r_H as a function of time and at a scattering angle of 120° by using PCS. From first mixing to first measurement an elapsed time of less than 10 s occurred. The sample time (incremental division of total measurement duration) and photon count signal to the correlator were continually readjusted throughout the reaction in accordance with the rate of aggregate growth and changing scattered intensity. The initial sample time was set between 18 and 20 μs. Individual PCS samples (i.e., each determination of a hydrodynamic radius) were made as rapidly as possible for the initial stages of DLA, with an average increase in measured radius of less than 5% between samples. Initial particle concentrations ranged between 6×10^{10} cm^{-3} and 5×10^{12} cm^{-3} and were varied to control the reaction rate and allow reasonable PCS determinations.

We measured the angular-dependent scattered intensity profile for a suspension of large aggregates after $I(q)$ became independent of time in the q range of interest, typically 4.6×10^{-3} to 2.6×10^{-2} nm^{-1} (20–160°), and for different aggregate sizes for both RLA and DLA. A minimum of five 3-s photon counts were made for

(35) Teixeira, J. In *On Growth and Form, Fractal and Non-Fractal Patterns in Physics*; Stanley, H. E., Ostrowsky, N., Eds.; Proc. NATO ASI Ser., Ser. E, No. 100; Martinus Nijhoff: Dordrecht, Netherlands, 1986; pp 145–162.

(36) Schaefer, D. W.; Martin, J. E.; Wiltzius, P.; Cannel, D. S. In *Kinetics of Aggregation and Gelation*; Family, F., Landau, D. P., Eds.; Proc. Int. Top. Conf.; Elsevier Science: Amsterdam, 1984; pp 71–74.

(37) Rarity, J. G.; Pusey, P. N. In *On Growth and Form, Fractal and Non-Fractal Patterns in Physics*; Stanley, H. E., Ostrowsky, N., Eds.; Proc. NATO ASI Ser., Ser. E, No. 100, Martinus Nijhoff: Dordrecht, Netherlands, 1986; pp 218–221.

(38) Martin, J. E. *J. Appl. Crystallogr.* **1986**, *19*, 25.

(39) Weitz, D. A.; Lin, M. Y. *Phys. Rev. Lett.* **1986**, *57*, 2037.

(40) Meakin, P.; Family, F. *Phys. Rev. A* **1987**, *36*, 5498.

(41) Ball, R. C.; Weitz, D A.; Witten, T. A.; Leyvraz, F. *Phys. Rev. Lett.* **1987**, *58*, 274.

(42) Weitz, D. A.; Huang, J. S.; Lin, M. Y.; Sung, J. *Phys. Rev. Lett.* **1985**, *54*, 1416.

(43) Martin, J. E. *Phys. Rev. A* **1987**, *36*, 3415.

(44) Cornell, R. M.; Mann, S.; Skarnulis, A. J. *J. Chem. Soc., Faraday Trans. 1* **1983**, *79*, 2679.

(45) Parfitt, R. L.; Russell, J. D.; Farmer, V. C. *J. Chem. Soc., Faraday Trans. 1* **1976**, *72*, 1082.

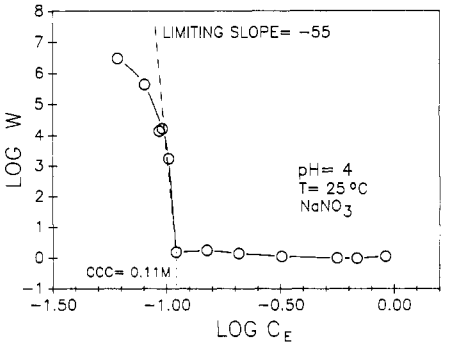

Figure 1. Stability curve for α-FeOOH in $NaNO_3$ at pH 4. Extrapolation of the stability ratio (W) to log $W = 0$ (···) gives the critical coagulation concentration (CCC) in mol·L^{-1} and determines the point of transition from reaction-limited (C_E < CCC) to diffusion-limited (C_E > CCC) aggregation.

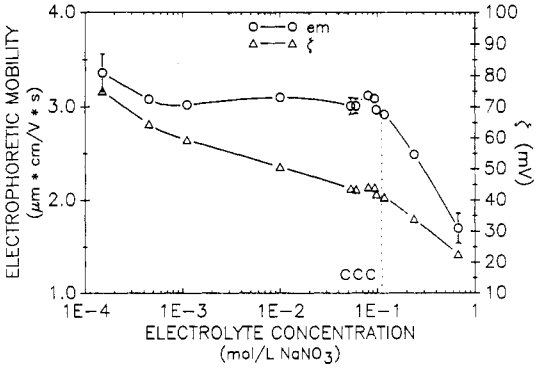

Figure 2. Electrokinetic behavior of α-FeOOH at pH 4. Electrophoretic mobility (em) and ζ potential (ζ) are plotted as a function of $NaNO_3$ concentration. Error bars on em curve represent the sample deviation. (···) critical coagulation concentration.

each q and then averaged and corrected for dark count, correlator dead time, and changes in scattering volume. We measured the electrophoretic mobility of these samples after completing SLS profiles. In addition, we carried out separate studies of particle mobility as a function of aggregate size and particle concentration.

Results and Discussion

Stability. Results of the aggregation kinetics study are summarized in the form of a stability curve in Figure 1. These data clearly indicate the existence of two limiting kinetic regimes. The CCC determined from this plot is 0.11 M, above which the aggregation rate is independent of C_E, and in this rapid growth region the rate is limited only by the particle diffusion time (DLA). Below the CCC the aggregation rate decreases with decreasing C_E as predicted by DLVO theory, and the rate is reaction-limited (RLA). A pronounced bending of the stability curve at low C_E may be an effect of sample polydispersity[30] or may be due to the large uncertainties associated with measuring aggregation times of several weeks duration. Also from Figure 1, the limiting value for d log W/d log C_E is −55, a relatively large slope reflecting the rapid transition from highly stable to destabilized sol over a very narrow range in C_E. Considering the experimental error involved in the determination of W, and the increasing curvature at low C_E, this estimate has approximately a ±40% margin of uncertainty, allowing a range in slope still well above the typical values[30,46] (≈5–15) measured for spherical particles.

Figure 2 shows a plot of electrophoretic mobility (em) as a function of C_E measured over a broader range than is attainable in a kinetic experiment. We find em is relativey insensitive to C_E over almost 3 decades in the RLA region, with a well-defined transition occurring near the CCC. In a separate study it was determined that, within the range of this study, em is independent of cluster size but is dependent on particle mass-concentration for C_E > 0.09 M, where em increases with concentration, approaching an asymptotic limit at around 50 mg·L^{-1}. The effect becomes more pronounced at higher C_E, being particularly strong above the CCC. We currently believe this to be an instrumental aberration related to the low signal intensity and lower mobility of these samples and for this reason use only em values determined in the asymptotic limit. Further studies may elicit a more specific cause for this anomaly.

We convert em to ζ with a modified version of the O'Brien and White[47] program and use the measured r_H = 39 nm as an effective radius. This calculation method assumes a spherical geometry and must therefore be considered as an approximation for asymmetric G2 particles. To our knowledge no similar method has been derived for flat plates. Van der Woude et al.[21] compared results obtained on spheroidal and plate-like goethite using the O'Brien and White procedure and found satisfactory agreement, except at small κr, where distortions of the double layer due to particle shape are most probable. Results from the present study are plotted with em in Figure 2. Note that, in contrast to em, ζ is a monotonically decreasing function of C_E, with only a small divergence near the CCC. It would appear that em is a more practical indicator of the onset of instability in this system. The low-C_E portion of the potential curve gives dζ/d log $C_E \approx$ 10 mV, increasing to 24 mV above the CCC. These slopes are in excellent agreement with reported values for oxide systems and typically lie well below the 60-mV Nernstian response predicted by Gouy–Chapman–Stern-type models.[48]

Using eq 9 and 12, and an aggregation potential of 41.4 mV, we calculate an effective A_{212} equal to 4.1×10^{-20} J. This is roughly the same value we derive from the reported data of Van der Woude et al.[21] for a similar goethite suspension at pH 2, and it is in the typical range for clay colloids.[28] Alternatively, one may determine A_{212} by systematic variation of its value in eq 10 in conjunction with eq 7–9 and by use of the appropriate values for the CCC, until $U_{max} = 0$ as determined graphically from potential energy curves generated as a function of separation distance. Applying this method we obtain $A_{212} = 3.7 \times 10^{-20}$ J, and the corresponding DLVO potential energy diagram for a series of C_E is shown in Figure 3a, where the electrostatic screening effect is apparent in the progression from curve a to i. The area of interaction used in generating these curves was determined from TEM dimensions 60 nm × 18 nm ($S = 1.08 \times 10^{-15}$ m^2) characterizing the dominant (100) face of G2. A plate thickness δ = 11 nm was chosen as an approximation based on TEM imaging and BET surface area analysis.

Figure 3a also illustrates some of the general features of DLVO energy curves: (1) a deep primary minimum at small separation distances (these curves ignore Born repulsion occurring at atomic distances), (2) a weak secondary minimum at longer distances, and (3) a potential maximum at some intermediate distance. Small particles such as G2 are not ordinarily subject to secondary minimum coagulation. For irreversible aggregation to occur,

(46) Shaw, D. J. In *Introduction to Colloid and Surface Chemistry*, 2nd ed.; Butterworths: London, 1978; Chapter 8, pp 167–232.
(47) O'Brien, R. W.; White, L. R. *J. Chem. Soc., Faraday Trans. 2* **1978**, *74*, 1607.
(48) Hunter, R. J.; Wright, H. J. L. *J. Colloid Interface Sci.* **1971**, *37*, 564.

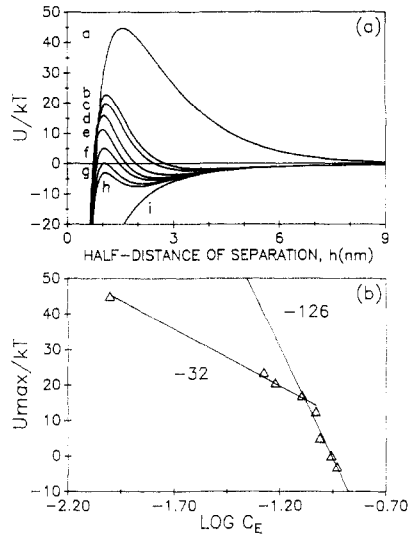

Figure 3. DLVO energy of interaction for α-FeOOH at pH 4. (a) Total potential energy (U), in thermal energy units (kT), is plotted as a function of the half-separation distance between plates and electrolyte concentration. Curves: (a) 0.01 M, (b) 0.053 M, (c) 0.06 M, (d) 0.08 M, (e) 0.093 M, (f) 0.097 M, (g) CCC = 0.11 M, (h) 0.117 M, (i) 0.237 M. (b) Potential energy maximum as a function of log electrolyte concentration for curves a through h.

approaching particles must have sufficient kinetic energy to overcome the potential barrier and reach the primary minimum, while the potential maximum acts as an activation energy for this process. Long-term kinetic stablity is attained at low C_E when $U_{max} \geq$ about $10–15kT$.[33] Generally, the DLVO theory is in qualitative agreement with experimental observations.

Figure 3b is a plot of U_{max}/kt as a function of log C_E for each interaction curve. Two limiting slopes are indicated from this data; however, the larger value (slope = −126) pertains to the range in C_E used in the experimental determination of d log W/d log C_E and should therefore be more applicable for comparative purposes. The calculated slope (−126) in this case is more than a factor of 2 larger than the experimental slope (−55). Theoretically, the magnitude of the slope is independent of A_{212} but proportional to ψ_S.[30] Although there are several sources of error in the determintaion and use of ζ as an approximation for ψ_S, for this region of C_E, where $\kappa r > 1$, these errors are expected to be very small, while the changes in ζ necessary to bring the slopes into agreement are relatively large. The slope is also proportional to S, the surface area of interaction. Van der Woude et al.[21] suggested a nonparallel particle interaction model to account for the lower experimental slope they measured for platelike goethite particles. In their hypothesis, S is reduced through initial edge or crosswise contact, followed by realignment into a parallel position. For the G2 system, also platelike, a reduction in S to about 40% of the initial value is necessary for a good fit to the experimental stability slope, and this is reasonably close to the expected surface area for crosswise interaction.

Structure. Static scattering curves were determined for aggregated suspensions of G2 covering a range in electrolyte concentration from 0.09 to 0.7 M and for r_H in the range from ~250 to ~1500 nm. Before these results are interpreted, it is important to establish the dilute nature of scattering in these systems. Extinction measurements were performed on highly aggregated suspensions up to the largest particle concentration used, and it was determined that at 632 nm less than 20% of the light is extinguished over a 1-cm cell path at the high concentration, and less than 2% is extinguished for the unaggregated suspension. These results indicate that the Born approximation for weak scattering[49] is valid in these systems and allows us to rule out multiple scattering effects.

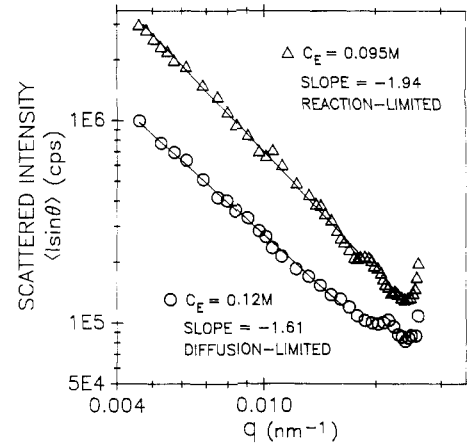

Figure 4. Static scattering profiles for aggregated α-FeOOH. Scattering exponents are determined from the slope of the linear portion of these curves. For visibility, reaction-limited curve is shifted vertically by a factor of 2.5 × I sin θ.

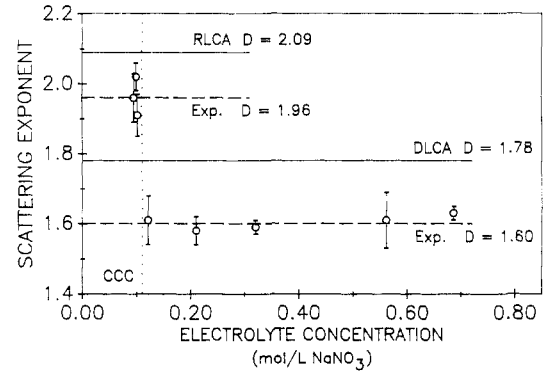

Figure 5. Scattering exponents (x) for aggregated α-FeOOH as a function of electrolyte concentration. Fractal interpretation gives x = fractal dimension (D). RLCA, reaction-limited cluster–cluster aggregation model; DLCA, diffusion-limited cluster-cluster aggregation model; Exp., experimentally measured average; (···) critical coagulation concentration.

Figure 4 shows two representative scattering profiles for rapid and slow aggregation conditions. The fractal dimension (scattering exponent) was determined from the low-q slope in the region where $qR > 1$, and the results are summarized in Figure 5. It is apparent from these plots that two types of structures are formed with D = 1.96 and 1.60 for RLA and DLA, respectively. The concentration at which a transition in structure occurs is coincidental with the CCC, represented in Figure 5 by a vertical dotted line. Above ζ = 41 mV the aggregates are formed under conditions of low sticking probability (s) and are relatively compact (larger D) in comparison to the highly ramified structures formed when the electrostatic repulsion is sufficiently screened ($U_A > U_R$).

Much insight can be gained from a comparison of these experimental findings with computer simulations of simple kinetic growth models for colloidal aggregation. The diffusion-limited cluster–cluster model (DLCC) of Meakin[50] and of Kolb, Botet, and Jullien[51] simulates random aggregation with Brownian (random-walk) trajectories and

(49) Wilcoxon, J. P.; Martin, J. E.; Schaefer, D. W. *Phys. Rev. Lett* **1987**, *58*, 1051.
(50) Meakin, P. *Phys. Rev. Lett.* **1983**, *51*, 1119.
(51) Kolb, M.; Botet, R.; Jullien, R. *Phys. Rev. Lett.* **1983**, *51*, 1123.

a sticking probability $s = 1$. In the lattice version of DLCC, a fixed concentration of monomers (occupied sites) is randomly distributed on a d-dimensional lattice and allowed to mutually diffuse. Cluster–cluster and particle–cluster interactions are permitted, and irreversible sticking occurs when two occupied sites are adjacent (nearest-neighbor occupancy). This model generates structures with $D \approx 1.8$ in 3-d and has universal properties with respect to microscopic details such as diffusion coefficient and lattice symmetry.[52] Rapid aggregation experiments on spherical gold[53,54] and silica[55] colloids are in agreement with these simulations, suggesting 1.8 is an effective dimensionality for DLA. The reaction-limited variant of the cluster–cluster model[40,56] (RLCC), in which s tends to zero, yields a value of D close to 2. Weitz and co-workers[39,42] have studied RLA through controlled additions of pyridine to initiate slow aggregation of citrate-stabilized gold colloids, and they find $D \approx 2.1$, in good agreement with RLCC. Similar results for RLA have been found with silica[36,43,55] and polystyrene microspheres.[37] Theoretically, it is the fractal dimension of the walk (d_w) or particle trajectory that ultimately determines the value of D for a given system. The crookedness of the Brownian path ($d_w = 2$) in DLA results in a high interception probability between mobile clusters, causing them to stick (on contact) mostly at the tips or perimeter sites with very little interpenetration occurring.[2] As growth continues by the process of smaller clusters combining to form larger clusters, much open space is left behind in the interior regions. This screening effect is responsible for the highly ramified nature of DLA aggregates. In RLA, the motion which brings clusters and particles together remains Brownian, but because of a repulsive barrier at short interaction distances, s approaches zero, and clusters can randomly sample many orientational possibilities before sticking. The effective particle trajectory is zero dimensional[40] ($d_w = 0$) since the clusters have an equal probability of sticking in any configuration, and interpenetration and branch thickening result in a more compact fractal structure with a higher dimensionality. Generally, as d_w is decreased, D increases with a corresponding increase in compactness ($D = d$ represents a completely compact structure).

Results from the present study yield a D that is significantly lower than the expected DLA value as discussed above. This may indicate that some additional factor is influencing the aggregation process in this system. There may be several possible sources for this deviation. (1) Size effects: When the ratio R/r is small, the scattering profile may be subject to finite size effects,[35] which tend to lower the scattering exponent and underestimate D. Additionally, in off-lattice 3-d simulations of DLCC,[57] D increased asymptotically with cluster size, although D was always >1.7. We find no dependency of D on R for G2 aggregates in the size range studied ($6 < R/r < 37$), however, we do not entirely rule out size effects. (2) Anisotropic sticking effects: Some investigators have reported low values for D in 3-d[58,59] and 2-d[60] aggregation experiments and have attributed these results to polarization effects. Recent extensions of the DLCC model have included electrostatic polarizability[61] and dipolar magnetic interactions[62] to account for the experimentally observed behavior, and both of these lead consequently to a reduction in D due to a preferred tip-to-tip sticking orientation, with values close to $D = 1.4$ in 3-d. We cannot reconcile the physical basis for these models with the G2 (DLA) system, for which electrostatic interactions are fully screened and the particles are antiferromagnetic with no net magnetic moment. However, the concept of anisotropic sticking (e.g., tip-to-tip) does have some physical significance for G2 particles which are platelike in shape and have a demonstrated tendency to aggregate, over relatively short length scales, in a face-to-face orientation. The Witten-Sander (WS) aggregation model[63] has been used to investigate the effect of anisotropic sticking on the structure of DLA clusters in 2-d[64,65] with the finding that anisotropy tends to decrease D. Although the WS model in 2-D (immobile cluster growing by a single particle addition) is not strictly representative of real colloidal aggregation (cluster–cluster growth) in 3-d, WS does incorporate some basic kinetic processes associated with DLCC, and we might expect a somewhat similar trend in the latter.

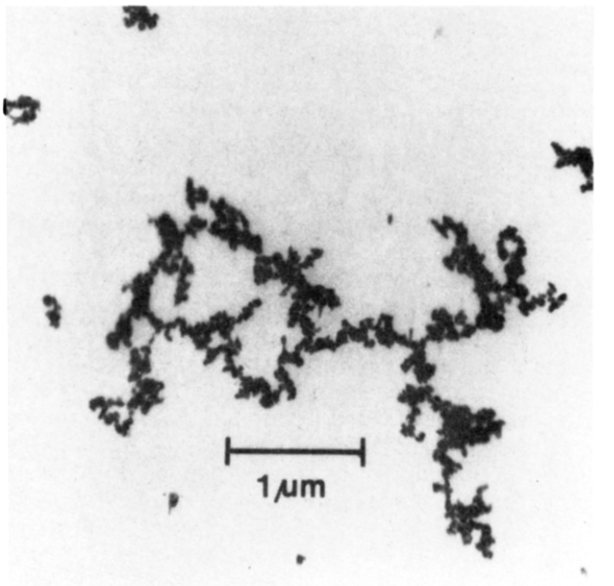

Figure 6. Transmission electron photomicrograph of α-FeOOH aggregated under diffusion-limited conditions at high electrolyte concentration. The "string-like" ramified structure is indicative of fractal growth under these conditions.

Anisotropic sticking is a plausible explanation for the low D measured for G2 aggregates, and we propose a simple model to account for this influence. In the DLA regime, electrostatic repulsive forces are screened, and the strongest attractive potential between particles would exist when the predominant (100) faces are parallel, providing a maximum surface area of interaction (see eq 10). Under these conditions, anisotropy, in the form of a preferred face-to-face orientation, is a response to short-range (<20 nm) van der Waals attractive forces acting between particles. As an aggregate grows linearly, however, the randomness of the process and the increasing surface area perpendicular to the axis of growth promote the formation

(52) Meakin, P.; Wasserman, Z. R. *Phys. Lett.* **1984**, *103A*, 337.
(53) Weitz, D. A.; Oliveria, M. *Phys. Rev. Lett.* **1984**, *52*, 1433.
(54) Weitz, D. A.; Huang, J. S. In *Kinetics of Aggregation and Gelation*; Family, F.; Landau, D. P., Eds.; Proc. Int. Top. Conf.; Elsevier Science: Amsterdam, 1984; pp 19–28.
(55) Aubert, C.; Cannell, D. S. *Phys. Rev. Lett.* **1986**, *56*, 738.
(56) Jullien, R.; Kolb, M. *J. Phys. A: Math. Gen.* **1984**, *17*, L639.
(57) Meakin, P. *Phys. Lett.* **1985**, *107A*, 269.
(58) Axelos, M.; Tchoubar, D.; Bottero, J. Y.; Fiessinger, F. *J. Phys. (Paris)* **1985**, *46*, 1587.
(59) Kim, S. G.; Brock, J. R. *J. Colloid Interface Sci.* **1987**, *116*, 431.
(60) Hurd, A. J.; Schaefer, D. W. *Phys. Rev. Lett.* **1985**, *54*, 1043.
(61) Jullien, R. *J. Phys. A: Math. Gen.* **1986**, *19*, 2129.
(62) Mors, P. M.; Botet, R.; Jullien, R. *J. Phys. A: Math. Gen.* **1987**, *20*, L975.
(63) Witten, T. A., Jr.; Sander, L. M. *Phys. Rev. Lett.* **1981**, *47*, 1400.
(64) Meakin, P. *Phys. Rev. A* **1986**, *33*, 3371.
(65) Meakin, P.; Chen, Z.; Evesque, P. *J. Chem. Phys.* **1987**, *87*, 630.

of a fractal structure by the normal clustering-of-clusters process. The resulting clusters have the tenuous nature of DLCC, but with the short-range ordering that strengthens the 1-d aspect of branches and lowers the effective dimensionality on length scales analyzed in our scattering experiments. Indeed, from TEM imaging (see Figure 6) we have noted the occurrence of relatively long 1-d ("string-like") branches in DLA aggregates. A more extensive TEM analysis has not been performed due to the persistent problem of preparation artifacts (particularly in the low C_E samples). There exists some disparity between the present interpretation and that of Van der Woude et al.,[21] primarily concerning our conclusion that RLA aggregates should appear more compact than DLA (a generally excepted condition) and that the latter are in fact more, not less, "string-like" than the former, as evidenced by the lower scattering exponent. Since the aforementioned authors do not discriminate between length scales in their observations, it is difficult to make further comparison.

One might predict a transition in the long-range correlations of larger clusters when the 1-d segments are small in size relative to R, and the DLCC dimensionality is recovered. The mechanism outlined above would not affect the spherically symmetric particles used in previous investigations. Furthermore, in RLA this effect is not as evident in $S(q)$ because electrostatic forces dominate the particle trajectory, although short-range ordering may still manifest itself in a manner previously described, in which restructuring occurs subsequent to edge or crosswise contact into the primary minimum, as postulated by Van der Woude et al.[21]

Short-range ordering is expected to have a significant effect on chemical processes occurring at the particle/solution interface. For instance, Anderson et al.[1] have studied the adsorption of phosphate onto goethite and find evidence of site burial and oscillatory uptake which they attribute to ordered aggregation. Short-range structure may also influence the physical properties of clusters,[66] in particular the susceptibility and response to shear-induced reorganizational processes. Some evidence of restructuring has been found in the G2 DLA system for very large aggregates ($R > 1500$ nm) aged for 2 h or more. In this case, an increase in the slope of the scattering curve, beginning at high q and moving toward low q with time, indicates that the clusters are approaching a more compact structure with $D > 2$. Restructuring to a higher dimensionality has been reported by other investigators,[55,66] although in those systems the slope of the scattering curve either increased at low q or steepened from low q to high q. Simulations[67] of 3-d DLCC with contact point reorganization following each aggregation event result in an increase of D from 1.80 to 2.09, in good agreement with experimental results. Restructuring processes are not well understood at the present time, and much work is needed to form a clearer picture of this phenomenon.

Conclusions

In summary, we have reported on an investigation of the salt-induced aggregation of colloidal iron oxide in aqueous suspension, using primarily nondestructive in situ light-scattering techniques. Quasi-elastic measurements of the initial aggregation rate indicate two kinetic regimes in which growth is either diffusion- or reaction-limited. The particle electrokinetic behavior reflects the influence of electrostatic interactions on reaction-limited aggregation, and DLVO stability theory calculations qualitatively illustrate the combined effects of van der Waals attractive and electrostatic repulsive forces on the kinetics. Measurements of the static structure factor as a function of momentum transfer reveal that the aggregates have long-range fractal correlations. The fractal dimension has different values for diffusion- and reaction-limited aggregation ($D \approx 1.6$ and 2.0, respectively), indicating different structures are formed depending on the kinetics involved. The value $D = 1.6$ is significantly lower than the typical diffusion-limited value $D = 1.8$ determined from model simulations and previous experimental work and may be a consequence of anisotropy in sticking. We postulate a simple model to explain this effect, in which short-range van der Waals forces are maximized by face-to-face interaction of plate-like goethite particles in the absence of repulsive forces. This mechanism leads to linear growth on short to intermediate length scales, thus lowering the effective dimensionality. The effect is diminished in reaction-limited aggregation, where the particle interactions are dominated by repulsive forces and the dimensionality of the particle trajectory is equal to zero.

This study demonstrates the need for further experimental work and model simulations focusing on the effects of short-range interactions on aggregate structure. Continuing investigations in this laboratory focus on short-range structure, specific adsorption effects on growth/structure, and reorganizational processes.

Acknowledgment. V.A.H. expresses his gratitude to Paul Meakin and Alex Nagel for helpful discussions concerning fractal concepts. This work was supported by the National Science Foundation through grant No. ECE-8504276.

Registry No. α-FeOOH, 20344-49-4; $NaNO_3$, 7631-99-4.

(66) Dimon, P.; Sinha, S. K.; Weitz, D. A.; Safinya, C. R.; Smith, G. S.; Varady, W. A.; Lindsay, H. M. *Phys. Rev. Lett.* **1986**, *57*, 595.

(67) Meakin, P. *Adv. Colloid Interface Sci.* **1988**, *28*, 249.